Available online at www.sciencedirect.com
ScienceDirect
Journal of Nuclear Materials 376 (2008) 98–107
journal of nuclear materials
www.elsevier.com/locate/jnucmat

Effects of the microstructure and alloying elements on the iodine-induced stress-corrosion cracking behavior of nuclear fuel claddings

Sang Yoon Park *, Jun Hwan Kim, Myoung Ho Lee, Yong Hwan Jeong

Advanced Core Materials Lab, Korea Atomic Energy Research Institute, 150 Doekjin-dong, Yuseong-gu, Daejeon 305-353, Republic of Korea

Received 20 August 2007; accepted 4 January 2008

Abstract

A quantitative analysis of the iodine-induced stress-corrosion cracking (ISCC) process for a Zircaloy-4 cladding and a ZIRLO cladding was performed to support grain-boundary pitting coalescence (GBPC) and pitting-assisted slip cleavage (PASC) models for an ISCC behavior. It was focused on the effects of the microstructure on a grain-boundary pitting and the transgranular cracking phenomenon during a crack propagation step. Also, a microscopic analysis of the stress intensity applied to pits on a grain surface was performed to evaluate the cleavage crack propagation rate of the stress-relieved (SR) and re-crystallized (RX) grains. During the ISCC cracking, it was revealed that the grain shape and cleavage habit plane played important roles in a grain cracking, which resulted in an IG–TG_c (TG cracking by cleavage) or a TG_f (TG cracking by fluting)–TG_c cracking mode. An IG–TG_c cracking took place for the RX microstructure through a GB pitting, however, a TG_f–TG_c cracking did occur for the SR one which in turn increased its propagation rate. The increase of the pitting resistance at the grain-boundary played a critical role in the crack propagation rate of the ZIRLO cladding.

1. Introduction

Nowadays, most nuclear power reactors are adopting a high burn-up to increase their fuel economy, where the refueling cycle of the fuel bundles is extended. As the fuel burn-up increases, the diameter of the cladding decreases, while the outer diameter of the fuel pellet increases. Eventually the pellet and the cladding contact each other after some cycles have elapsed. During burn-up, the concentration of iodine inside fuel rod gradually increases and causes iodine-induced stress-corrosion cracking (ISCC).

The nucleation and the propagation of an ISCC crack is very complex to be fully understood. Recently, it has been proposed that grain-boundary pitting coalescence (GBPC) and pitting-assisted slip cleavage (PASC) models are appropriate for modeling crack nucleation and growth in fuel claddings, such as a commercial grade of nuclear fuel cladding [1,2]. The main factors affecting the crack initiation step are pitting nucleation, growth and agglomeration in that the pits are preferentially formed around a grain-boundary (GB) as a result of a local corrosion reaction by iodine. When these pits combine in a crystallographic slip plane, a cleavage crack is generated in that grain. Up to K_{ISCC}, a micro-crack is mainly grown by a GBPC, and above K_{ISCC}, this crack is quickly propagated by a PASC. GBPC and PASC models have successfully explained the ISCC behavior of Zircaloy-4 [1]. These models, however, need to be supplemented from some aspects, such as the effect of the microstructure and an alloying element on transgranular (TG) cracking by the PASC model. In addition, the reason why the re-crystallized (RX) structure has a lower crack propagation rate than a stress-relieved (SR) one or why an Nb-containing cladding has a higher ISCC resistance, has not been clearly explained. This study is aimed at supporting these models by using a quantitative and microscopic analysis of ISCC test results as well as detailed observations of the fractured surfaces of a

* Corresponding author. Tel.: +82 42 868 8597; fax: +82 42 862 0432.
E-mail address: nsypark@kaeri.re.kr (S.Y. Park).

0022-3115/$ - see front matter © 2008 Elsevier B.V. All rights reserved.
doi:10.1016/j.jnucmat.2008.01.024

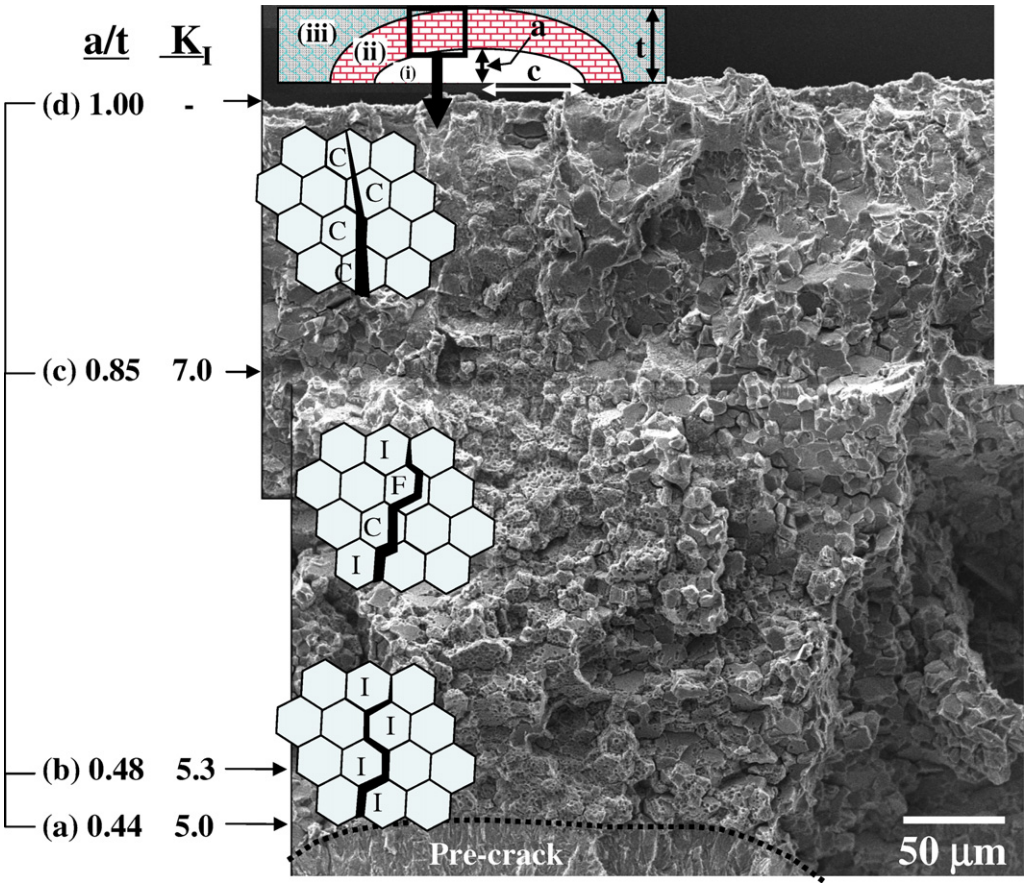

Fig. 1. Fractographs and fracture modes of an ISCC crack for the re-crystallized Zircalloy-4 cladding pressurized in an iodine environment at 350 °C; (i) fatigued pre-crack, (ii) ISCC, (iii) ductile fracture after test; I = IG, C = TG by cleavage, F = TG by fluting.

pre-cracked cladding tube, especially, the effects of the microstructure and an alloying element were focused on.

2. Experimental procedure

The specimens for this study were cut from a commercial grade low-tin Zircaloy-4 (Zr–1.3Sn–0.2Fe–0.1Cr) and ZIRLO cladding (Zr–1.0Nb–1.0Sn–0.1Fe). Their outer and inner diameters were 9.50 mm and 8.36 mm, respectively. Their length was 130 mm. They were all in as-received states in a stress-relieved condition. To investigate the effect of the microstructure, a specimen was heat-treated at 620 °C for 3 h to have a fully re-crystallized structure then it was used for the ISCC test. A specimen with an initial pre-crack was used in the test. A pre-crack was created by the fatigue cracking method which Lemaignan [3] employed.

Test specimen was put inside an autoclave, and then a medium, which was pure argon mixed with iodine, was pressurized inside the cladding after reaching a constant test temperature of 350 °C. The iodine used in this study, which had a purification of 99.99%, was supplied by Aldrich.[1] The iodine concentration was kept constant at 1.5 mg/cm^2. After the test, the specimen was examined using a scanning electron microscope (SEM) to determine the actual crack propagation depth during the ISCC test, and then the crack propagation velocity was calculated. The ISCC crack propagation rate with respect to the applied K_I was evaluated to determine the threshold stress intensity factor (K_{ISCC}). The K_I value was adjusted so that the stress state around the crack tip was in a plane strain condition. The detailed experimental procedure regarding a fatigue pre-cracking and the ISCC procedure can be found in previous papers [1,2].

[1] Aldrich Chemical Company, Inc., Milwaukee WI 53233 USA.

3. Results

3.1. Effect of the microstructure

Fig. 1 shows the schematic crack shape, crack propagation mode and SEM fractographs of a fully re-crystallized (RX) Zircaloy-4 specimen which was pre-cracked and pressurized at 145 MPa for 12.3 h in an iodine environment. In the early stage, the crack was propagated by an intergranular (IG) ISCC cracking, in the later stage, however, the crack propagation mode was switched to a cleavage-like transgranular (TG) cracking. And, in the intermediate stage, both a TG and an IG were observed. According to

the GBPC model, the pits were preferentially formed on the GB and grew into a micro-crack which initiated an IG crack. To evaluate the effect of a micro-crack on the initiation of an ISCC crack, SEM fractography was performed at a position far from the pre-crack. Fig. 2 shows the morphologies of the fractured cross-section far from the pre-crack position. It shows that a group of pitting clusters was developed in the IG crack which acted as initiation sites for an ISCC.

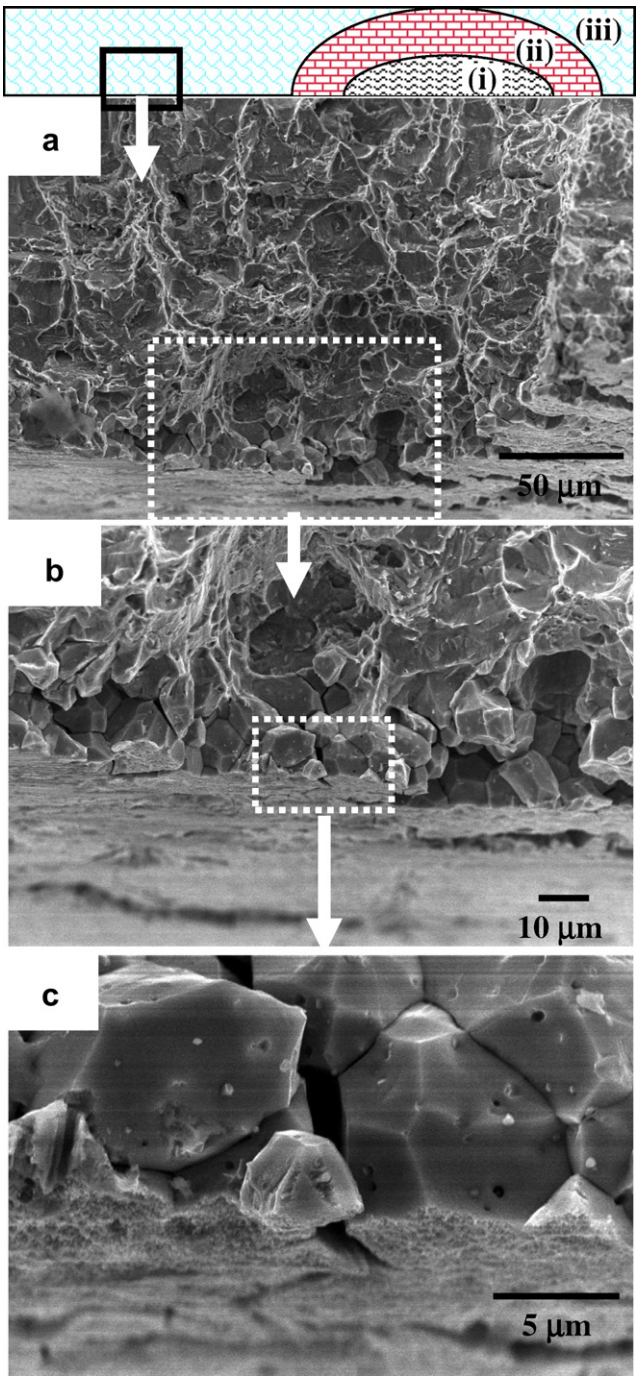

Fig. 2. Morphologies of the fractured cross-section far from the pre-crack showing the crack initiation site for the RX cladding pressurized in an iodine environment; (a) 500X, (b) 1000X, and (c) 5000X.

Fig. 3 shows the schematic crack shape and SEM fractographs of a stress-relieved (SR) Zircaloy-4 specimen which was pre-cracked and pressurized at 173 MPa for 10 min in an iodine environment. And Fig. 4 shows high magnification SEM photographs of an ISCC crack. In general, the fractured surface of the SR condition shows an axially elongated microstructure which was cracked after a fluting and cleavage caused by a TG cracking.

Fig. 5 shows the comparisons of the stress intensity factor and the rupture time between the SR and RX structures, which were tested in the conditions of Fig. 1 and Fig. 3. Although the difference of the pre-crack dimension and stress intensity factor was less than 35%, the rupture time of the RX cladding was 80 times larger than that of the SR cladding.

3.2. Effect of an alloying element

Fig. 6 shows the fractographs of the re-crystallized Zircaloy-4 and ZIRLO claddings for the ISCC crack surface. It was pressurized in an iodine environment at 145 MPa for 12.3 h in the case of the Zircaloy-4 cladding and at 172 MPa for 22.3 h in the case of the ZIRLO cladding. For the Zircaloy-4, both IG and TG cracks were observed at the same time, showing that a lot of pits and pitting clusters were developed on the IG surfaces. The size of the pits was less than 2 μm. Regarding the TG surfaces, however, no pits were shown. The figure also shows that the majority of the GBs are severely attacked by pitting. For the ZIRLO cladding, both IG and TG cracks were observed at the same time. In this case, the pits were fine and shallow and could be seen on the whole surface. Contrary to the result of Zircaloy-4, the GB of the ZIRLO cladding is not attacked by a pitting corrosion.

Fig. 7 shows the fractographs of the RX claddings near the interface between an ISCC crack and a ductile fracture. The a/t (defined in Fig. 1) value and the parametric angle of the observation point of the elliptical crack were about 0.8 and 45°, respectively. For Zircaloy-4, only TG cracks, according to cleavage and fluting, were observed with no micrometer scale pits. The high magnification photos showed only small and shallow pits. For the ZIRLO cladding, IG cracks were rarely observed, however, some crystallographic surfaces were selectively attacked by nanometer scale pits (Fig. 7 (e) and (f)).

3.3. Threshold stress intensity factor

Fig. 8 shows the crack propagation rate of the Zircaloy-4 and ZIRLO claddings with SR and RX structures with respect to the applied K_I. For Zircaloy-4, re-crystallization increased the ISCC resistance such that the K_{ISCC} value of the SR and RX specimens were 3.3 and 4.8 MPa $m^{0.5}$, respectively, in addition, the crack propagation rate in region II was reduced by 10 times for the RX condition when compared to that of the SR condition. For the ZIRLO cladding, however, no difference was found between

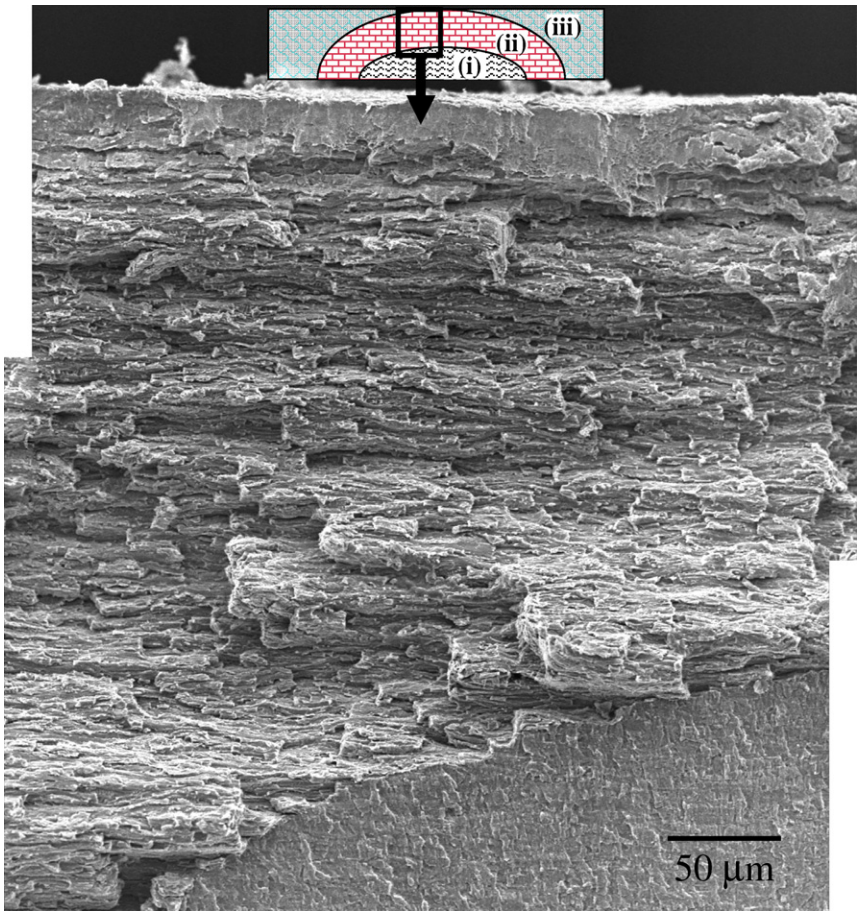

Fig. 3. Fractographs of an ISCC crack for the stress-relieved Zircaloy-4 cladding pressurized in an iodine environment at 350 °C; (i) fatigued pre-crack, (ii) ISCC, (iii) ductile fracture after the test.

the SR and RX specimens from this study, resulting that the K_{ISCC} value or the crack propagation rate of the RX and SR specimens have a similar value.

4. Discussions

4.1. Crack propagation mechanism

Recently, GBPC and PASC models have been proposed to explain the ISCC crack initiation and propagation mechanism of a Zircaloy-4 surface. This is depicted in Fig. 9 [2]. Fig. 2 clearly shows an ISCC crack initiation by a GBPC mechanism on the inner surface. The ISCC crack is nucleated by pits at first and they cluster with each other along the grain-boundary, and then the crack grows by an IG mode during an early step of a cracking. In Fig. 1, the crack's growth by an IG cracking was continued until the a/t ratio reached 0.48.

In the intermediate step ($a/t = 0.48$–0.85 for Fig. 1), however, the crack is propagated by a mixed IG and TG mode, as shown in Fig. 1 and Fig. 6. In this region, a TG crack that passed through one grain cannot penetrate further into a neighboring grain so that it changes its direction along the grain-boundary to show an IG crack along several grains. A crack by the TG mechanism will appear after some IG cracks have preceded it. The TG crack takes place according to the following mechanism.

(1) The pits are formed on the grain surface during the early stage of an IG cracking by the iodine attack, which grow and coalesce with each other to develop into a microcrack.
(2) If the pits (micrometer scale) and associated microcracks are arranged on the line of a cleavage habit plane of a grain (Fig. 6(b)), a cleavage crack takes place at a low stress intensity ($K_I = 5.3$–7.0 MPa $m^{0.5}$ at Fig. 1).
(3) If a habit plane of a neighboring grain does not become parallel to that of a TG-cracked grain and the stress intensity is low, then the cleavage does not continue to the neighboring grain, and the cleavage is stopped at the GB.
(4) IG crack continuously accumulates to induce the next cleavage crack.
(5) If the crack depth becomes large enough, a cleavage crack takes place only through a nanometer scale pitting because of a high K_I value (Fig. 7).

It is generally known that a TG crack in Zircaloy would propagate in parallel to a basal plane [4–8]. But Peehs et al.

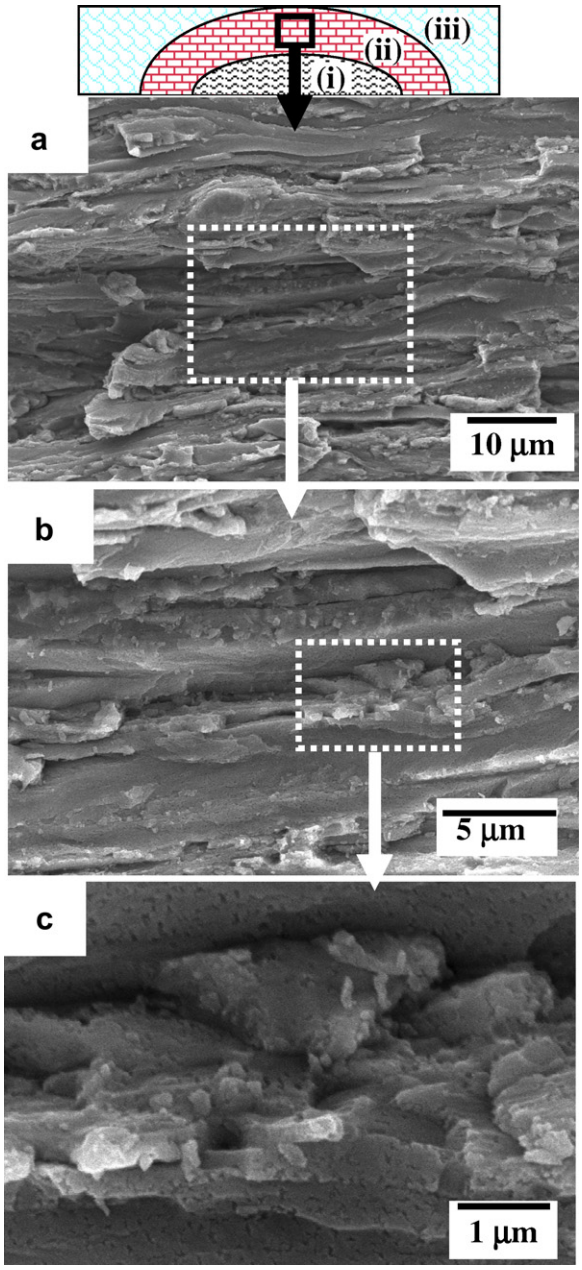

Fig. 4. Fractographs of an ISCC crack for the SR Zircaloy-4 cladding pressurized in an iodine environment at 350 °C; (i) fatigued pre-crack, (ii) ISCC, (iii) ductile fracture after the test.

[9] reported that such a crack would propagate easily in a 50–70° direction to a basal plane. Cox [4] also reported that a TG crack would propagate along a slippery prism plane as well as a basal plane. Both basal and slippery prism planes could be habit planes for a cleavage TG crack. The reason why a TG crack arrests in a grain and cannot penetrate further into a neighboring grain is that the applied K_I value is too low to induce the next TG crack.

In a later step ($a/t = 0.85$–1.0 for Fig. 1), a crack was propagated by a cleavage-like TG cracking, which passed through one grain to a neighboring grain without changing its direction. This is because such a crack has a deep depth

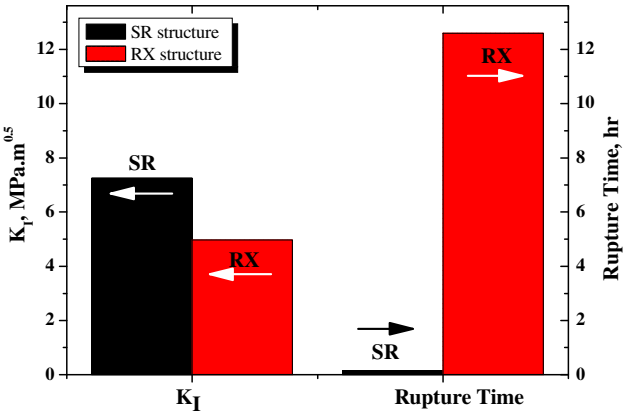

Fig. 5. Comparisons of the stress intensity factors and rupture times between the SR and RX structures, which were tested in the conditions of Fig. 1 and Fig. 3.

at this step and its stress intensity at its crack tip is so high that a cleavage cracking can take place without the aid of a PASC or a selective crystallographic plane. Because a crack caused by a TG exhibits a continuous cleavage-like fracture surface, the crack propagation rate at this stage is very high.

4.2. Effects of the microstructure on the PASC model

When the K_I value reaches a threshold K_{ISCC} represented by the growth of an IG cracking, such a crack rapidly propagates with the aid of a PASC mechanism. As shown in Fig. 3 and Fig. 4, the crack propagates by a TG mode with a fluting and a cleavage for the SR Zircaloy-4 [1,10–12]. In the high magnification fractographs (Fig. 4), a cleavage and a fluting was clearly seen and they were arranged in an alternate position, and nanometer scale pits were formed on the whole fracture surface. It means that a cleavage took place by the action of nanometer scale pits in spite of a low K_I. In addition, the TG cracking behavior depended on the microstructure.

Fig. 10 shows schematic illustrations of the surface crack formed on the SR and RX grain surfaces by a pitting cluster in order to simulate the effect of a pitting cluster on a crack propagation at a TG boundary, as in Fig. 6(b). The grain volume of the RX and SR grains are assumed to be the same, which are $6 \times 6 \times 6\ \mu m^3$ for RX and $30 \times 2.4 \times 3\ \mu m^3$ for SR, respectively. Newman and Raju [13] has presented a stress intensity factor equation for semielliptical surface cracks in finite elastic plates subjected to tension or bending loads. We tried to use this equation for Fig. 10. Fig. 11 shows the stress intensity boundary-correction factor ($K_I/S_t\sqrt{\pi a/Q}$) applied at the surface crack in Fig. 10. Although a uniform tension and bending moment can be applied to a surface crack, the bending moment term is excluded from this calculation for simplicity. The dimensions of the surface crack were selected in the range of $a/c = 0.2$–0.8 and $a/t = 0.05$–0.5 as shown in Table 1. In spite of the same size of the surface crack, the stress

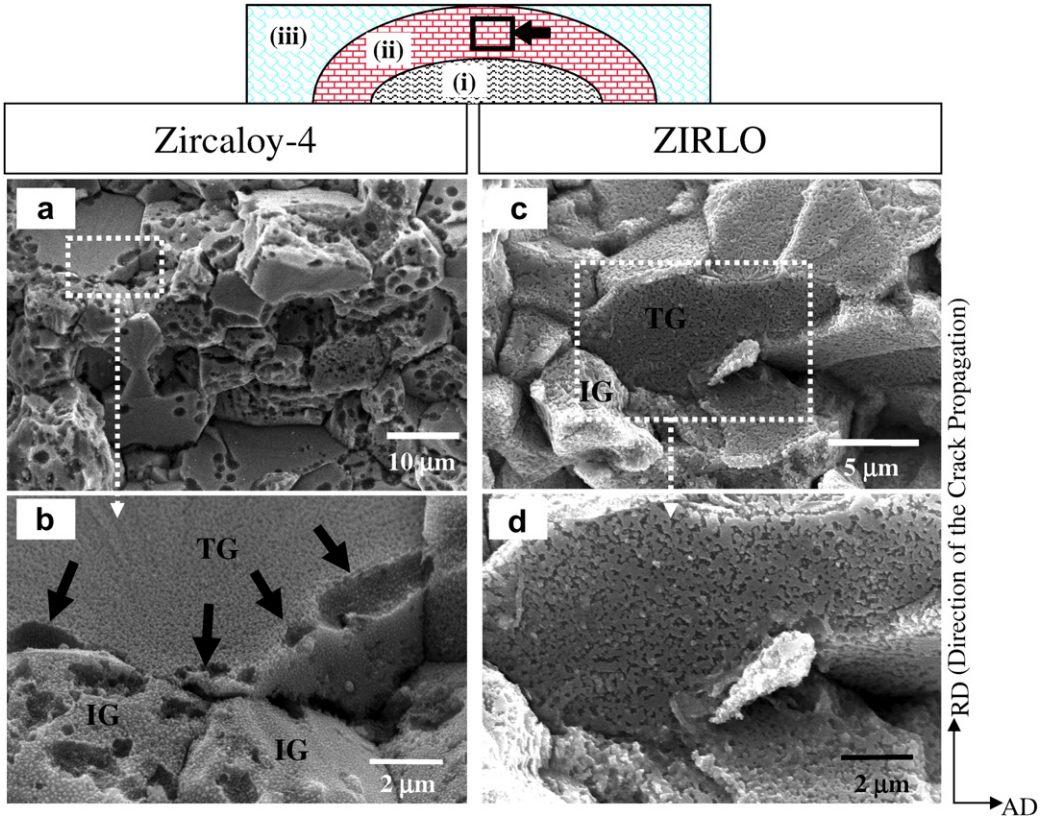

Fig. 6. Fractographs of an ISCC crack for the RX Zircalloy-4 and the RX ZIRLO cladding pressurized in an iodine environment at 350 °C; (a) and (b) Zircaloy-4 (arrows show the pits or pitting clusters formed on the GB of TG-cracked grain), (c) and (d) ZIRLO cladding.

intensity of the SR grain is always higher than that of the RX grain. The larger the surface crack is, the higher the stress intensity factor applied to the SR grain along the $\varphi = 0$ direction is, which means the possibility of a cleavage cracking increases in the case of the SR grains. Since the laminar type SR grains have a larger value of a/t than that of the RX ones, their surface crack in the SR structure suffers from higher stress intensity than that in the RX one. In spite of the small pits or a surface crack of a nanometer scale, the a/t value in the SR grain is so large that it can initiate a cleavage or fluting. If a surface crack becomes parallel to a cleavage habit plane, a cleavage cracking takes place in the grain. Otherwise, a fluting crack takes place in the grain.

On the other hand, the a/t value of an equiaxed RX grain is so small that a cleavage or fluting cannot take place in the grain with the aid of a nanometer scale pitting, because the stress intensity boundary-correction factor on the pitting is very small even if the stress at the RX grain surface is the same as the SR one. When the pits on the RX grain surface become a micrometer scale as shown in Fig. 6(b), a cleavage cracking takes place in the grain with the aid of the PASC mechanism in spite of a low K_I. Therefore the crack propagation rate of the RX microstructure is lower than that of the SR one. If the stress intensity factor increases with the macro-crack depth, as in Fig. 7, a considerable fluting and cleavage takes place in spite of a nanometer scale pitting.

4.3. Effects of an alloying element

Fig. 6(c) and (d) show the SEM fractographs of the fully re-crystallized (RX) ZIRLO cladding that was pre-cracked and pressurized at 172 MPa for 22.3 h in an iodine environment. Both IG and TG cracks can be observed on the fractured surface, however, large pits (micrometer scale) or pitting clusters cannot be seen on the entire surface. Only small (nanometer scale) and shallow pits were formed on both the IG and TG surfaces. The IG surface was severely attacked by many pits for the Zircaloy-4 (Fig. 6(a) and (b)), but not for the ZIRLO cladding. It means that the GB of the Zircaloy-4 has a lower pitting resistance than that of ZIRLO in an iodine environment. Therefore, a GB of Zircaloy-4 can be damaged easily by a pitting which causes a TG cracking with the aid of the PASC mechanism. Because of this TG cracking mode, Zircaloy-4 has a high crack propagation rate.

The high stress intensity allows the grain to become cleaved or fluted with the aid of nanometer scale pits by a PASC mechanism, where the crack propagates with a TG_f (TG by fluting)–TG_c (TG by cleavage) mode. The crack propagates with a IG–TG_c mode in a low stress intensity, because a cleavage takes place ahead of a fluting on the cleavage habit plane. Fig. 6 shows the IG–TG_c mode crack with a low stress and Fig. 7 shows the TG_f–TG_c mode crack with a high stress. For the ZIRLO cladding, the IG mode was rarely observed at a high stress as shown in Figs. 7(e) and (f).

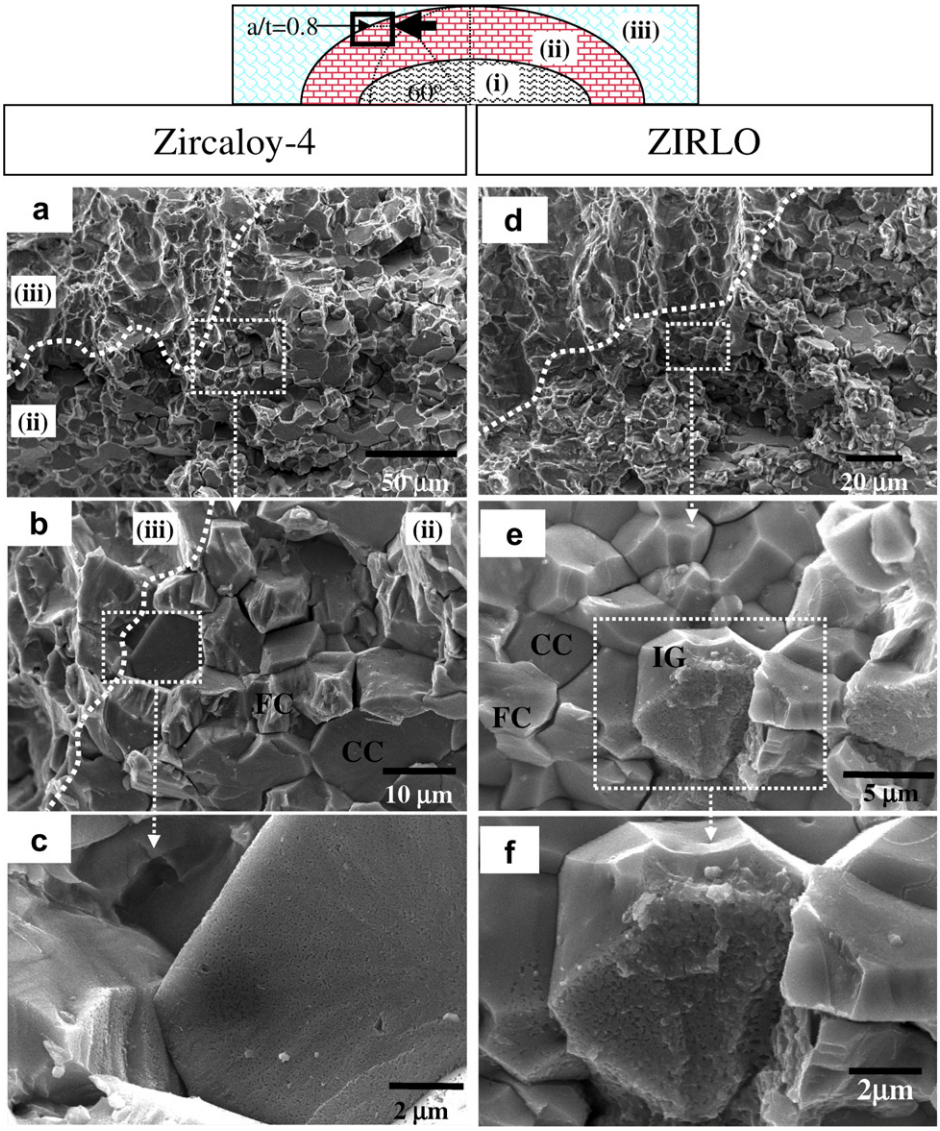

Fig. 7. Fractographs of the RX Zircaloy-4 and of the RX ZIRLO cladding near an interface between an ISCC fracture and a ductile fracture; (a) and (b) Zircaloy-4, (c) and (d) ZIRLO cladding.

Table 2 shows the K_{ISCC} and the crack propagation rate at $K_I = 6$ MPa $m^{0.5}$, calculated from Fig. 8. They show reasonable results which coincide well with the GBPC and PASC mechanisms. Because the grain size of the RX Zircaloy-4 is larger than that of the RX ZIRLO cladding, the K_{ISCC} and the propagation rates of them are similar to each other in spite of a difference in the GB pitting resistance.

4.4. Effects of the crystallographic plane

As mentioned in the previous section, the GB surface of RX Zircaloy-4 has many pits of micrometer scale, but not the TG surface. Also a cleaved and fluted plane of the SR Zircaloy-4 as shown in Fig. 4 does not have any micrometer scale pits. It seems that its pitting resistance largely depends on the crystallographic plane.

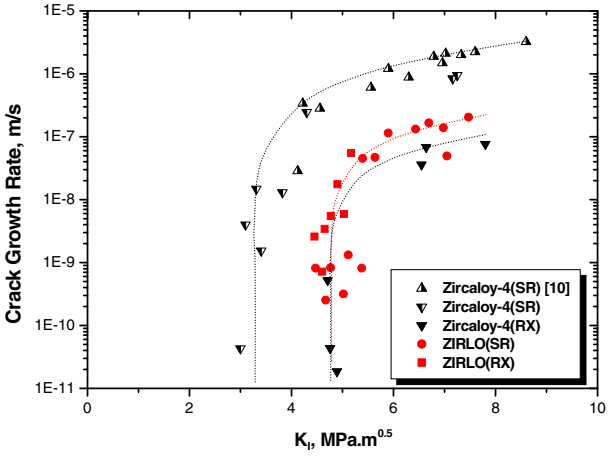

Fig. 8. Plots of da/dt vs. K_I for the Zircaloy-4 and ZIRLO cladding.

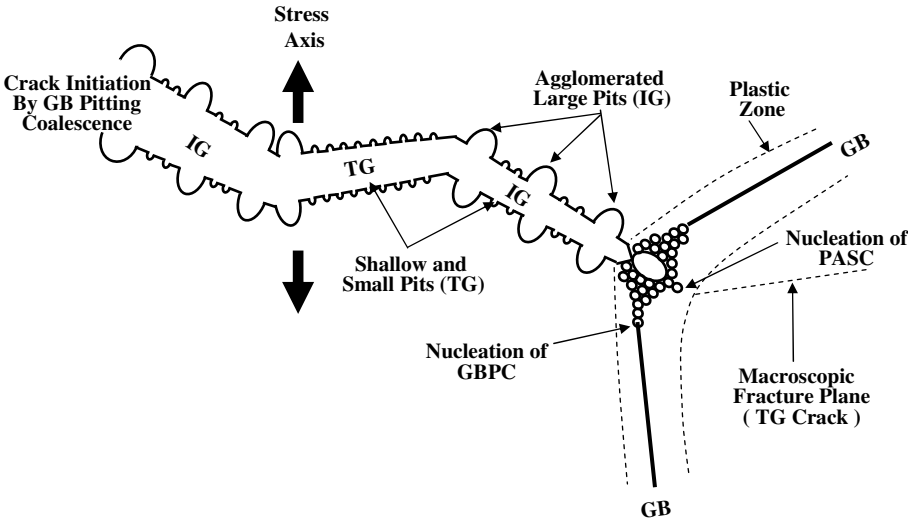

Fig. 9. Schematic diagram showing an ISCC crack initiation/propagation by the grain-boundary pitting coalescence (GBPC) and pitting-assisted slip cleavage (PASC) models [2].

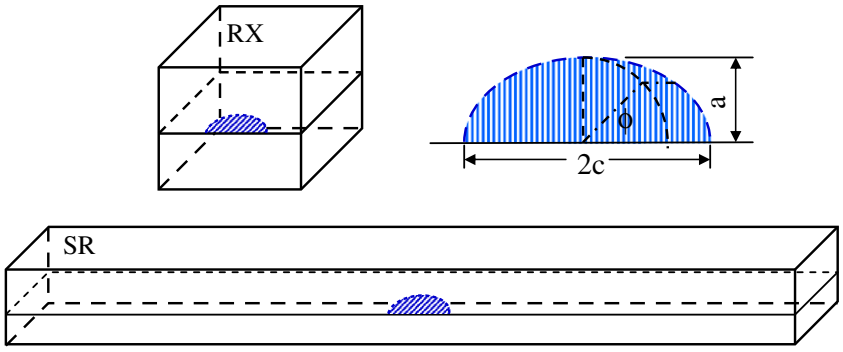

Fig. 10. Schematic diagrams of the surface crack formed by the GBPC mechanism on the SR and RX grain surfaces.

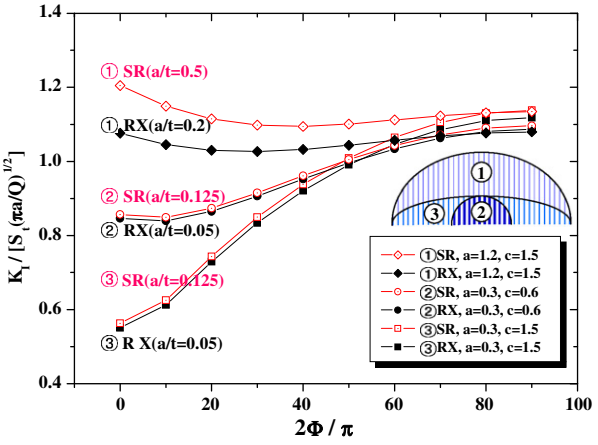

Fig. 11. Typical results of the stress intensity factors for the surface crack formed by the GBPC mechanism on the SR and RX grain surfaces.

When iodine is adsorbed into the zirconium cladding, the zirconium bond at the grain-boundary (GB) will be weakened, so its surface energy will be reduced [5,14]. In

Table 1
Comparisons of the surface crack dimensions on a grain with the SR and RX structures

No.	Micro-structure	a	c	t	a/c	a/t
1	SR	1.2	1.5	2.4	0.8	0.5
	RX	1.2	1.5	6	0.8	0.2
2	SR	0.3	0.6	2.4	0.5	0.125
	RX	0.3	0.6	6	0.5	0.05
3	SR	0.3	1.5	2.4	0.2	0.125
	RX	0.3	1.5	6	0.2	0.05

Table 2
Comparisons of the stress intensity factors and crack propagation rates between the SR and RX structures

Alloy	Microstructure	K_{ISCC} (MPa $m^{0..5}$)	da/dt (at 6 MPa $nf^{0.5}$) (m/s)
Zircaloy-4	SR	3.4	1.34×10^{-6}
	RX	4.8	6.62×10^{-8}
ZiRLO	SR	4.8	1.04×10^{-7}
	RX	4.8	1.04×10^{-7}

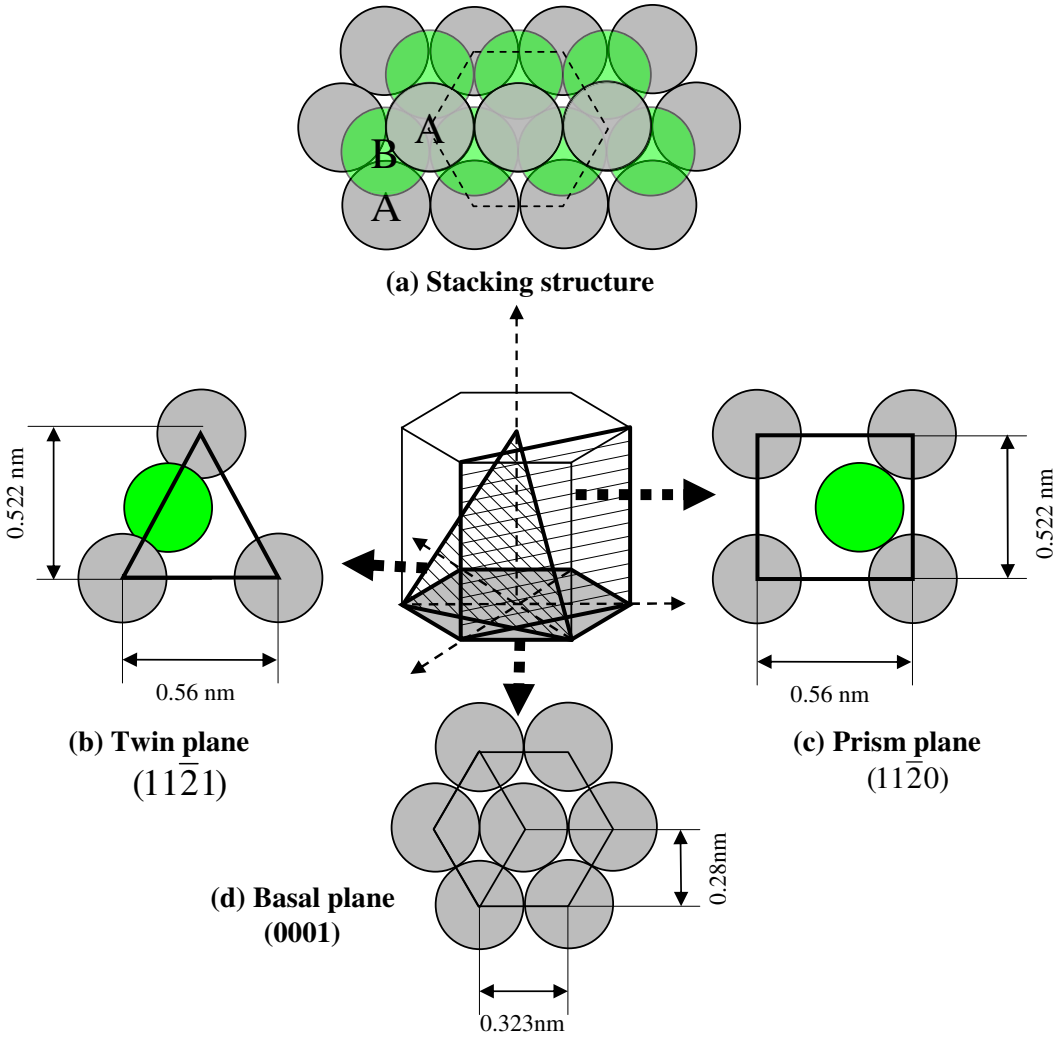

Fig. 12. Schematic diagram of the stacking structure and hexagonal planes in zirconium; (a) stacking structure, (b) twin plane (11$\bar{2}$1), (c) prism plane (11$\bar{2}$0), (d) basal plane (0001).

addition, any free iodine can react with the zirconium to form solid iodides and a gaseous zirconium tetra-iodide (ZrI_4) [15]. This gaseous ZrI_4 can be decomposed easily into the iodine and Zr at a strained surface by an applied hoop stress, thus pits are formed due to a localized attack on the GB. Therefore, the adsorbability of the iodine atom on the Zr-alloy can be explained in terms of the iodine diffusivity into the Zr-alloy [16].

Fig. 12 shows schematic illustrations of the stacking structure and crystallographic planes of the Zr-alloy. The iodine atoms on the specimen with a (0001) plane can diffuse through the closely packed basal plane, while the iodine atoms on the other planes diffuse through non-closely packed planes. The iodine diffusion rate primarily depends on the planar atomic density of the diffusion plane. These findings strongly indicate that the planar atomic density and atom array of a plane play a critical role in the pitting kinetics, and have a considerable influence on the pitting morphology and on the cleavage habit plane. From this point of view, the basal plane has the lowest adsorbability for the iodine atom and the prism plane has the highest. A pitting, therefore, is formed well on a prism plane along a basal plane which is a cleavage habit plane.

In the early stage of a cracking, an ISCC crack nucleates at a grain-boundary by a GBPC mechanism that is purely an IG mode. During a crack growth and propagation, TG_c and TG_f modes take place with an increase of the stress intensity at a crack tip. TG_c takes place in low stress intensity with a GB pitting and a cleavage habit plane, however, a TG_f takes place in high stress intensity without the aid of a cleavage habit plane. For the SR microstructure, the stress intensity boundary-correction factor on the GB pitting is higher than that of the RX one because of its laminar type grain structure. Therefore TG_f–TG_c is the main factor for the cracking mode during the crack propagation for the SR microstructure, however, IG–TG_c is the main factor for the RX microstructure which reduces the propagation rate. So, the interactions among the stress intensity, the direc-

tion of the crystallographic plane, the pitting resistance at the GB and the grain shape play important roles in a crack propagation behavior.

5. Conclusions

From a quantitative and microscopic analysis of ISCC test results as well as detailed observations of the fractured surface of a pre-cracked Zircaloy-4 cladding and a ZIRLO Zr-cladding, the following can be summarized.

1. GBPC and PASC models have successfully explained the ISCC behavior in terms of the crack nucleation, initiation and propagation behaviors of Zircaloy-4 or ZIRLO cladding in an iodine environment.
2. When the K_I value of a crack reaches a threshold K_{ISCC}, the crack rapidly propagate. This main crack propagation step during an ISCC revealed that the grain shape and cleavage habit plane play important roles in a grain cracking by a GB pitting, which cause an IG–TG_c or TG_f–TG_c cracking mode. IG–TG_c mode occurs frequently in an RX microstructure. In the SR condition, on the other hand, the TG_f–TG_c mode appears frequently which increases the propagation rate.
3. An increase of the pitting resistance at a grain-boundary plays a critical role in decreasing the crack propagation rate of the ZIRLO cladding.

Acknowledgement

The work reported in this paper has been carried out under the Nuclear R&D program by MOST.

References

[1] S.Y. Park, et al., J. Nucl. Mater. 372 (2–3) (2008) 293.
[2] S.Y. Park, J.H. Kim, B.K. Choi, Y.H. Jeong, Met. Mater. Int. 13 (2007) 155.
[3] C. Lemaignan, Int. J. Pres. Ves. Piping 15 (1984) 241.
[4] B. Cox, J. Nucl. Mater. 172 (1990) 249.
[5] J.C. Wood, J. Nucl. Mater. 45 (1972) 105.
[6] R.L. Jones, D. Cubicciotti, B.C. Syrett, J. Nucl. Mater. 91 (1980) 277.
[7] B.C. Syrett, D. Cubicciotti, R.L. Jones, Nucl. Technol. 55 (1981) 628.
[8] R.B. Adamson, J. Nucl. Mater. 82 (1980) 363.
[9] M. Peehs, H. Stehle, E. Steinberg, in: Proceedings of the Fourth International Symposium on Zirconium in the Nuclear Industry, June 1978, Stratford-upon-Avon, England, ASTM STP-681, p. 244.
[10] D. Le Boulch, L. Fournier, C.S. Catherine, in: International Seminar on Pellet-cladding Interaction in Water Reactor Fuels, March 2004, Aix en Provence, France.
[11] C. Lemaignan, I. Schuster, in: Proceedings of the Technical Committee Meeting on Properties of Materials for Water Reactor Elements and Methods of Measurement, Vienna, Austria, 1986.
[12] I. Schuster, C. Lemaignan, J. Joseph, SMiRT-12C03/2 (1993) 45.
[13] J.C. Newman Jr., I.S. Raju, Eng. Fract. Mech. 15 (1981) 185.
[14] B. Cox, J. Nucl. Mater. 170 (1990) 1.
[15] D. Cubicciotti, R.L. Jones, B.C. Syrett, in: Zirconium in the Nuclear Industry, Boston, Mass, ASTM STP 754, 1982, p. 146.
[16] H.G. Kim, T.H. Kim, Y.H. Jeong, J. Nucl. Mater. 306 (2002) 44.